Li *et al. Molecular Cancer* (2024) 23:185
https://doi.org/10.1186/s12943-024-02080-1

Molecular Cancer

CORRESPONDENCE Open Access

The prognostic effect of infiltrating immune cells is shaped by proximal M2 macrophages in lung adenocarcinoma

Jian-Rong Li[1,2], Vikram Shaw[1], Yupei Lin[1,2], Xiang Wang[1,3], Muhammad Aminu[4], Yong Li[2,7], Jia Wu[4], Jianjun Zhang[5,6], Christopher I. Amos[1,2,7] and Chao Cheng[1,2,7*]

Abstract

The spatial arrangement of immune cells within the tumor microenvironment (TME) and their interactions play critical roles in the initiation and development of cancer. Several advanced technologies such as imaging mass cytometry (IMC) providing the immunological landscape of the TME with single-cell resolution. In this study, we develop a new method to quantify the spatial proximity between different cell types based on single-cell spatial data. Using this method on IMC data from 416 lung adenocarcinoma patients, we show that the proximity between different cell types is more correlated with patient prognosis compared to the traditional features such immune cell density and fractions. Consistent with previous reports, our results validate that proximity of T helper (Th) and B cells to cancer cells is associated with survival benefits. More importantly, we discover that the proximity of M2 macrophages to multiple immune cells is associated with poor prognosis. When Th/B cells are stratified into M2-distal and M2-proximal, the abundance of the former but not the latter category of Th/B cells is correlated with enhanced patient survival. Additionally, the abundance of M2-distal and M2-proximal cytotoxic T cells (Tc) is respectively associated with good and poor prognosis. Our results indicate that the prognostic effect of Th, Tc, and B cells in the tumor microenvironment is modulated by the nearby M2 macrophages. The proposed new method proposed can be readily applied to all single-cell spatial data for revealing functional impact of immune cell interactions.

*Correspondence:
Chao Cheng
chao.cheng@bcm.edu
[1]Institute for Clinical and Translational Research, Baylor College of Medicine, Houston, TX 77030, USA
[2]Section of Epidemiology and Population Sciences, Department of Medicine, Baylor College of Medicine, Houston, TX 77030, USA
[3]Department of Quantitative and Computational Biology, Baylor College of Medicine, Houston, TX 77030, USA
[4]Department of Imaging Physics, The University of Texas MD Anderson Cancer Center, Houston, TX 77030, USA
[5]Department of Thoracic/Head and Neck Medical Oncology, The University of Texas MD Anderson Cancer Center, Houston, TX 77030, USA
[6]Department of Genomic Medicine, The University of Texas MD Anderson Cancer Center, Houston, TX 77030, USA
[7]Dan L Duncan Comprehensive Cancer Center, Baylor College of Medicine, Houston, TX 77030, USA

Lung adenocarcinoma (LUAD), the predominant subtype of non-small cell lung cancer (NSCLC), continues to be a leading cause of cancer-related mortality despite progress in early detection and therapy [1]. The interaction between the tumor microenvironment (TME) and malignant cells is pivotal to cancer development, progression, and metastasis [2]. Accumulating evidence suggests that the abundance and composition of immune cells within the TME correlate with patient outcomes in lung cancer [3]. More recently, the spatial arrangement of these immune cells has been shown to significantly impact prognosis in lung and various other cancer types [4, 5], but these studies were limited to individual immune cell types or their spa-

tial relationships to cancer cells [6]. The advent of imaging mass cytometry (IMC), however, has revolutionized this field by profiling the immune landscape with single-cell resolution [7]. A notable study by Sorin et al. utilized this technique to analyze IMC data from 416 LUAD patients, providing detailed spatial information on cancer cells, endothelial cells, and fourteen immune cell types, including $CD163^+$ macrophages (M2), $CD163^-$ macrophages (M1), Cytotoxic T (Tc) cells, $CD4^+$ T helper (Th) cells, regulatory T (Treg) cells, other T cells (Tother), classical monocytes (Cl Mo), non-classical monocytes (non-Cl Mo), intermediate monocytes (Int Mo), natural killer (NK) cells, dendritic cells (DC), mast cells, neutrophils, and other unclassified immune cells [8].

In this study, we develop a novel method to quantify the spatial relationship between distinct cell types based on their distributions captured by IMC images. Specifically, to measure the proximity of one cell type to another (X→Y), we compute the distances from each Y cell to the nearest X cell, creating a vector of distances {d1, d2, …, dn}, where n denotes the count of Y cells present in the image. These distances were aggregated to establish a cumulative distribution function, the area under which was calculated as the proximity score (see Methods for details). The proximity score (X→Y) produces a value from 0 to 1, where a higher score (Proximity-Hi) indicates closer proximity of X cells to Y cells (Fig. 1a, b). It is important to note that this method anticipates asymmetric proximity scores for X→Y versus Y→X due to the directional nature of the measurement.

After removing three cell types (Int Mo, NK, DC) with low abundance (average fraction < 1%), we calculated the proximity scores of thirteen cell types to cancer cells in all images from Sorin IMC data. Univariable Cox regression analysis revealed a significant association between the proximity of Th, M2, and B cells to cancer cells and patient overall survival (OS) (Fig. 1c). Notably, a closer proximity of Th→Cancer and B→Cancer correlated with improved survival outcomes (Hazard Ratio HR < 1, $P < 0.01$), whereas a closer proximity of M2Mac→Cancer was associated with poorer survival (HR > 1, $P < 0.01$), in line with the known anti-tumor functions of Th and B cells [8, 9] and the pro-tumor roles of M2 cells [10]. Expanding our analysis to encompass all possible pairings among the thirteen cell types, we found that 10 out of the 169 combinations were significantly correlated with survival (Fig. 1d, e). For these significant cell-cell interactions (CCIs, e.g., X→Y), the pro- or anti-tumor functions of X cells may depend on their proximity to Y cells in the TME. Of note, the five most significant CCIs involve M2 macrophages (M2→Th, M2→Endothelial, M2→Tc, M2→Tother, M2→Treg), emphasizing the influence of M2 macrophage distribution within the TME on patient prognosis in LUAD. For instance, the most significant CCI is M2→Th, with a higher proximity score associated with a worse prognosis (HR = 12.1, P = 8e-5, Fig. 1g). When stratified using the median proximity as the cut-off, the high-proximity patients showed a significantly shorter survival time compared to the low-proximity patients (HR = 1.73, P = 1e-4, Fig. 1f). This result was further validated in the validation cohort consisting of 60 LUAD patients: the progressed patients showed significantly higher M2→Th proximity scores than the non-progressed patients (Supplementary Fig. 1).

Since the proximity metric for X→Y was calculated based on the distances of Y cells to the nearest X cells, we anticipated a high score when X cells have a higher abundance in an image. Consistent with this, the M2Mac→Th proximity indeed showed a positive correlation with the abundance of M2 macrophages ($R > 0.60$, Supplementary Fig. 2), but was not correlated to Th cell abundance ($R < 0.05$, Supplementary Fig. 3). In fact, the fraction of Th cells in immune cells was positively correlated with patient prognosis (HR = 0.13, P = 0.003, Fig. 1g), while the fraction of M2 macrophages had a weak negative correlation with prognosis (HR = 6.78, P = 0.08, Fig. 1g). We therefore performed multivariable Cox regression analysis, which affirmed the prognostic significance of M2Mac→Th proximity after adjusting for the Th and M2Mac fractions (HR = 11.08, P = 0.002, Fig. 1g). Next, we utilized both M2Mac→Th proximity and Th cell fraction to refine prognostic stratification in LUAD. Patients were categorized into four distinct groups based on a median cutoff: high Th fraction with high M2Mac→Th proximity (Th+Pro+), high Th fraction with low proximity (Th+Pro-), low Th fraction with high proximity (Th-Pro+), and low Th fraction with low proximity (Th-Pro-). Among these, the Th+Pro- group exhibited the longest OS, whereas the Th-Pro+group had the shortest OS (Fig. 1h). These findings indicate that the anti-tumor efficacy of Th cells can be compromised by the presence of proximal M2 macrophages.

To further explore the spatial influence of M2 macrophages on Th cell functions, we classified Th cells from IMC images into two groups: those proximal to at least one M2 macrophage within 30 pixels (~30 μm), which were denoted as M2-proximal Th cells, and those beyond this threshold, which were denoted as M2-distal Th cells (Fig. 2a). After calculating the fraction of these two subsets out of the total immune cell count in each image, we observed a marked contrast in their prognostic implications. The fraction of M2-distal Th cells displayed a positive association with patient prognosis (HR = 0.04, P = 6e-5), which was even more significant than the overall Th cell fraction (HR = 0.13, P = 0.003, Fig. 2b, c and Supplementary Fig. 4). Conversely, the fraction of M2-proximal Th cells did not show a significant relationship with prognosis ($P > 0.1$). A similar pattern

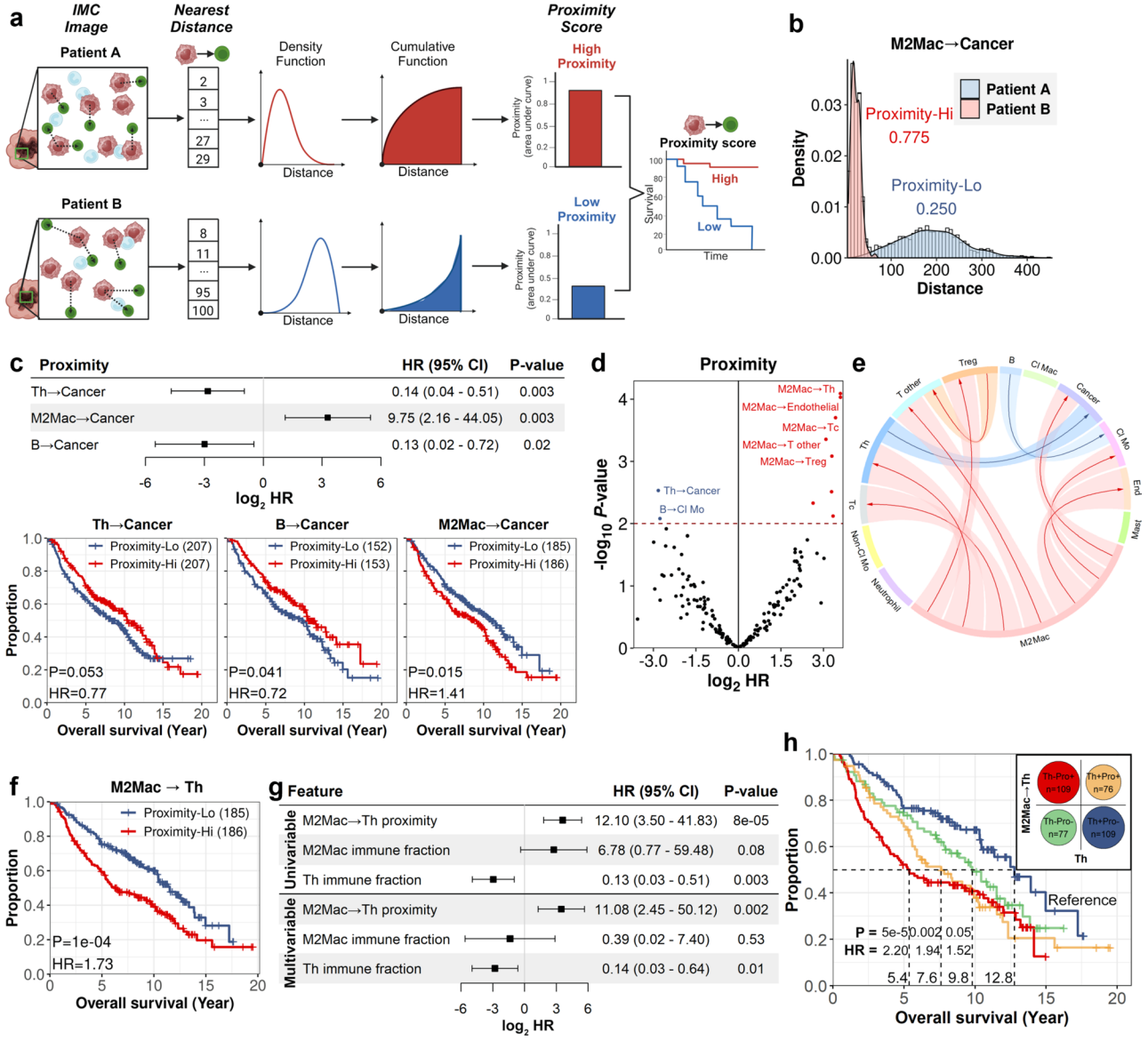

Fig. 1 The proximity between different cell types in the tumor microenvironment captured by IMC data is associated with patient prognosis in LUAD. (**a**) The schematic representation of the study framework. Within each IMC image, the distances of all Y cells to their nearest X cell are calculated, which are eventually transformed into a cumulative function. The area under this cumulative function yields a value between 0 and 1, defined as the proximity score from X to Y. Proximity scores for all combinations of cell types across all IMC images are utilized for prognostic analysis. *Created with BioRender.com.* (**b**) Illustrative examples of M2Mac→Cancer cell proximity in two LUAD IMC images, with a higher proximity score indicating a closer distribution of distances. (**c**) Among the 14 cell types analyzed for proximity to cancer cells, $CD4^+$ T cells (Th), M2 macrophages (M2Mac), and B cells demonstrated significant associations with overall survival (OS) of patients. (**d**) The volcano plot illustrates the prognostic associations of proximity scores for 169 pairs across 13 cell types. Univariable Cox regression analysis identified ten pairs of cell types with significant associations with prognosis. (**e**) A cell-cell interaction network formed the ten cell-cell pairs with significant prognostic associations. The direction of the arrows indicates the X→Y relationship, with red and blue arrows denoting a significant association with poorer and better prognosis, respectively. (**f**) Overall survival curves for LUAD patients categorized by high and low M2Mac→Th proximity scores (using the median as the cutoff). Patients with missing M2Mac→Th proximity score values were excluded from this analysis. (**g**) Univariable and multivariable Cox regression results for M2Mac→Th proximity score, M2Mac fraction in immune cells, and Th fraction in immune cells. (**h**) Overall survival curves for LUAD patients stratified by a combination of Th fraction and M2→Th proximity. Patients were categorized into four groups based on the median values of Th fraction and M2Mac→Th proximity: Th+ Pro+, Th-Pro+, Th-Pro-, and Th+ Pro-. The Th-Pro+ group exhibited a shorter median survival time of 5.4 years followed by Th+ Pro+ at 7.6 years, Th-Pro- at 9.8 years, and Th+ Pro- at 12.8 years. Note that M2Mac refers to $CD163^+$ macrophages and is abbreviated as M2Mac for figure readability

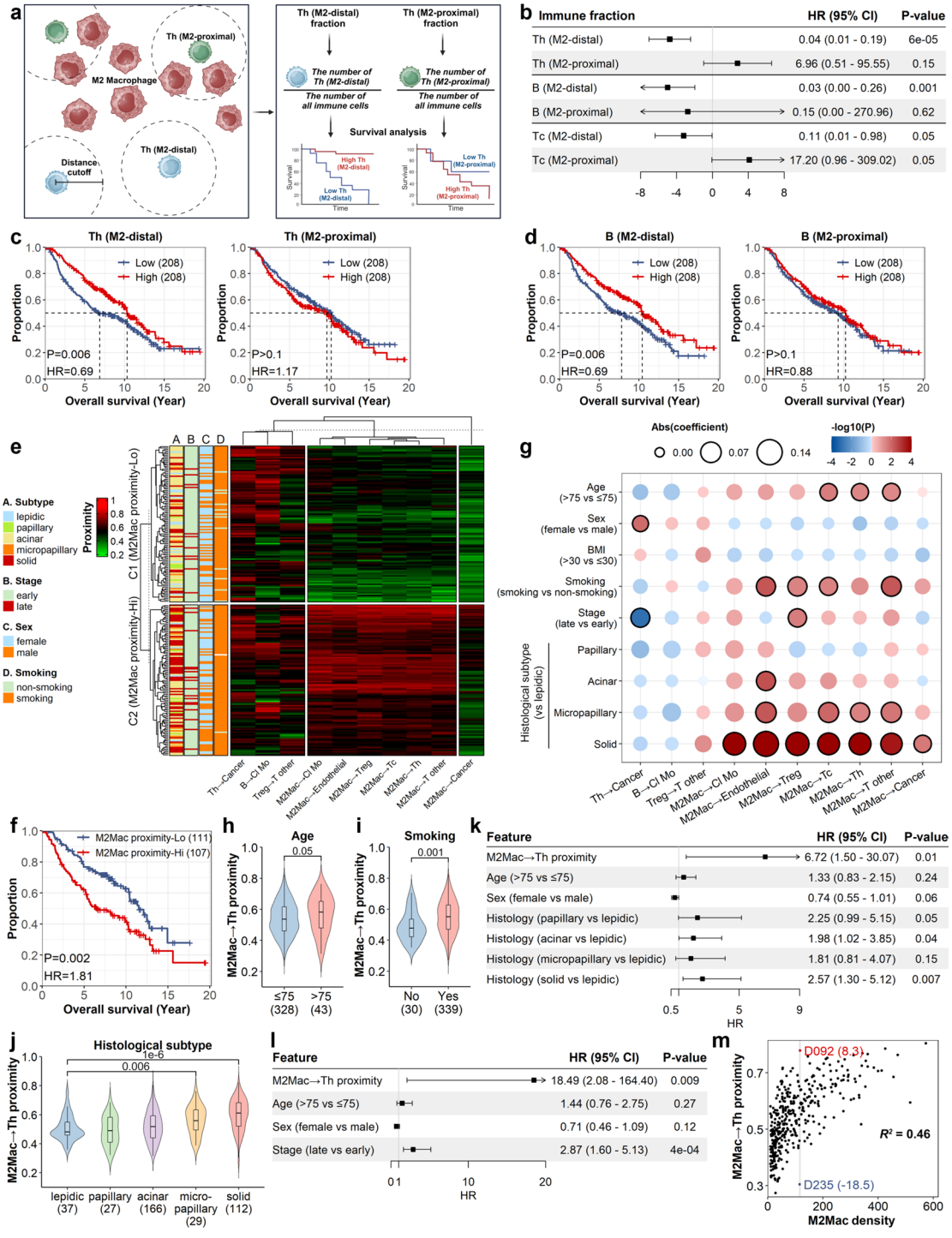

Fig. 2 (See legend on next page.)

was observed when B cells were stratified in the same way (Fig. 2b, d and Supplementary Fig. 4). When patients were divided into four groups based on the M2-distal Th and B cell fractions, the group with high fractions in both cell populations showed significantly better survival compared to the other three groups (Supplementary Fig. 5). Without stratification, the overall fraction of cytotoxic T cells (Tc) did not correlate with prognosis ($P>0.1$, Supplementary Fig. 4). Intriguingly, the fraction of M2-distal Tc was correlated with improved patient outcomes (HR=0.11, $P=0.05$), while the fraction of M2-proximal Tc was associated with worse prognosis (HR=17.2, $P=0.05$, Fig. 2b). These results were robust against the selection of neighborhood size (Supplementary Fig. 6).

(See figure on previous page.)

Fig. 2 Immune cells with and without M2 Macrophages in the neighborhood (M2-proximal versus M2-distal) show distinct prognostic correlations in LUAD. (**a**) Analytical framework illustration: $CD4^+$T cells (Th) in IMC images are categorized as M2-proximal Th if M2 macrophages are present within a 30-pixel radius, and as M2-distal Th if they are outside of that range. Survival analysis was conducted based on the fractions of M2-proximal and M2-distal Th cells in each IMC image. *Created with BioRender.com*. (**b**) Survival analysis results for the fractions of M2-proximal and M2-distal Th, B cells, and $CD8^+$T cells (Tc) within immune cells. (**c**) Overall survival curves for patients with high versus low M2-distal and M2-proximal Th fractions. (**d**) Overall survival curves for patients with high versus low M2-distal and M2-proximal B cell fractions. (**e**) Hierarchical clustering of the 10 prognostic immune cell pairs. (**f**) Overall survival curves for the two patient groups identified in the previous panel. (**g**) The correlations between the proximity scores for the 10 prognostic cell type pairs and clinical factors, including age, sex, smoking status, body-weight index (BMI), tumor stage, and predominant histological types. Dots surrounded by a black circle indicate statistical significance ($P < 0.01$). Red dots signify positive correlations, while blue dots indicate negative correlations. The size of each dot represents the magnitude of its coefficient calculated by the corresponding multivariable linear regression model. (**h**) Comparison of M2Mac→Th proximity in LUAD patients with age ≤ 75 versus those with age > 75. (**i**) M2Mac→Th proximity in smokers versus non-smokers. (**j**) M2Mac→Th proximity across five predominant histological subtypes in LUAD patients. (**k**) Multivariable Cox regression model adjusted for age, sex, and predominant histological subtype in early-stage (Stage I-II) LUAD patients. (**l**) Multivariable Cox model adjusted for age, sex, and stage in patients with a predominant histological subtype of acinar. (**m**) Scatter plot showing the correlation between M2Mac→Th proximity score and M2Mac density across IMC images. Each dot indicates an IMC image for a patient. Of note, we highlight two patients with similar M2Mac density but highly different M2Mac→Th proximity scores (0.779 for patient D092 versus 0.305 for patient D235). After adjusting for M2Mac density, the normalized proximity scores for them remain significantly different (8.3 for D092 versus − 18.5 for D235 = -18.5). R^2 indicates that M2Mac density explains 46% of the variation in M2Mac→Th proximity

Our findings underscore that M2 macrophages in the vicinity can significantly alter the prognostic impact of infiltrating Th, Tc, and B cells.

After establishing the prognostic relevance of cell proximity, we explored clinical factors that could influence the proximity between different cell types. A hierarchical clustering analysis based on the proximity scores of the 10 prognostic CCIs categorized LUAD samples into two distinct clusters (Fig. 2e). Notably, Cluster 2 exhibited a higher incidence of the solid histological subtype (49.5% versus 21.6%, P=2e-5, Fisher's exact test) and a lower proportion of non-smokers (0.9% versus 10.8%, P=0.003) than Cluster 1, with significant differences in survival outcomes between the clusters (HR=1.81, P=0.002, Fig. 2f). Next, we performed multivariable linear regression analysis using the proximity score as the dependent variable and various clinical factors as the independent variables, such as age, sex, smoking status, body-weight index (BMI), tumor stage, and predominant histological type (Fig. 2g). Interestingly, higher M2Mac→Th proximity scores were associated with patients over the age of 75 (Fig. 2h), smoking (Fig. 2i), and tumors classified as solid or micropapillary, compared to their counterparts with the lepidic subtype (Fig. 2j). These findings suggest that the proximity between cells was largely correlated with these factors.

As tumor stage and histological subtype are themselves well-established prognostic factors, we then examined whether the M2Mac→Th proximity score provides additional prognostic value. Multivariable Cox regression analysis revealed a moderate association of M2Mac→Th proximity with overall survival (OS) (HR=3.42, P=0.08, Supplementary Fig. 7), even after adjusting for age, sex, and histological subtype (BMI and smoking status were excluded due to a lack of prognostic association from univariable analysis). Since the majority of patients (n=365) in the IMC dataset presented with early-stage disease, we performed survival analysis within this subgroup. This analysis demonstrated the significant prognostic relevance of M2Mac→Th proximity after adjusting for age, sex, and histological subtype (HR=6.72, P=0.01, Fig. 2k). When we further dissected the data by histological subtypes, focusing on two major subtypes, acinar (n=190) and solid (n=118), a marked prognostic impact of M2Mac→Th proximity was observed for the acinar subtype (HR=18.49, P=0.009, Fig. 2l), but not for the solid subtype. These findings suggest that M2Mac→Th proximity may serve as a supplemental prognostic indicator, though it is highly correlated with tumor stage and histological subtype.

As above described, M2Mac→Th proximity and M2 macrophage abundance are highly correlated (R=0.68, Supplementary Fig. 2), suggesting that approximately 46% of the variation in proximity scores is attributable to the abundance of M2 macrophages. We rationalize that the remaining variation might be explained by interactions between cells in the TME, which may modulate molecular signaling (e.g., the interactions between cytokines and receptors). To explore the influence of molecular interactions on cell proximity, we randomly reassigned cell type labels in each IMC image while maintaining original cell counts and recalculated the proximity scores. This procedure was repeated 100 times to obtain the null distribution of proximity scores, which was then used for normalization. In this context, a positive normalized X→Y proximity score indicated that X cells are in closer proximity to Y cells than what was expected by chance. Conversely, a negative score would suggest a tendency for X cells to be more distant from Y cells than expected. Notably, after controlling for M2 macrophage density, we observed a partial correlation of 0.69 between M2→Th proximity and its normalized score (Supplementary Fig. 8), revealing that nearly half (48%) of the unexplained variation could be due to molecular interactions. For instance, in Fig. 2m we show two IMC images with similar M2 macrophage density but quite

different M2Mac→Th proximity scores (0.78 for sample D092 vs. 0.31 for sample D235). These two images vary substantially in their normalized proximity scores (8.3 for D092 vs. -18.5 for D235), suggesting that their proximity difference is mainly driven by molecular interactions.

In this study, we introduce a novel method to quantify the spatial relationship between distinct cell types based on their distributions captured by IMC images. Based on a similar concept, a few methods have been proposed to investigate the cell-cell interactions and spatial heterogeneity captured by IMC or multiplex immunohistochemistry (mIHC) images [11–13]. For example, Barua et al. proposed the G-cross function to measure the relative spatial distribution between different cell types [13]. When applied to the Sorin IMC data, this method achieved consistent results with our proximity analysis, but the prognostic association identified based on proximity scores tended to be more significant (Fig. 1d and Supplementary Fig. 9).

In the original study, Sorin et al. noted the prognostic association of B cells and the interactions of M2 macrophages with $CD8^+$ T and B cells [8]. Our analyses further reveal that the prognostic effect of these infiltrating immune cells is shaped by the proximity of M2 macrophages. As shown in Fig. 2b, the fractions of M2-distal but not M2-proximal Th and B cells are positively correlated with patient survival. More interestingly, the fractions of M2-distal and M2-proximal Tc cells showed positive and negative correlation with patient survival, respectively, which may explain why the prognostic association of Tc cells was not observed in the original report. M2 macrophages are known to play immunosuppressive roles in the TME and are implicated in the development and progression of cancer [10, 14]. In the TME, M2 macrophages impede $CD8^+$ T cells from engaging with tumor cells and reduce the effectiveness of anti-PD-1 treatments [15].

Although we demonstrated that the prognostic effect of key infiltrating immune cells can be influenced by the presence of M2 macrophages in the neighborhood, we did not explore the molecular alterations that mediate the functional variations between M2-distal and M2-proximal immune cells, which is a limitation of this study. Several advanced technologies, including 10x Genomics Visium HD, MERFISH, and GeoMx, have recently been employed for characterizing the TME of cancers. These methods provide spatial distributions of single cells and matched single-cell transcriptomic profiles. When data become available, further studies should investigate the molecular mechanisms by which the functions and states of immune cells are regulated by proximal M2 macrophages in LUAD and other cancers.

In conclusion, our analyses indicate that the spatial distribution between cells in the TME has a tremendous influence on their prognostic effect in LUAD. Particularly, the function of major immune cells such as Th, Tc, and B cells can be shaped by the proximal M2 macrophages.

Methods

The IMC dataset

The processed imaging Mass Cytometry (IMC) data and clinical information for a total of 416 patients with Lung Adenocarcinoma (LUAD) was generated by Sorin et al. and downloaded from https://doi.org/10.5281/zenodo.7383627. The IMC images, each covering a 1×1 mm² area, were processed to identify and mark cellular regions within the images, with each pixel representing approximately 1 μm². For each marked cell, the centroid serves as the cell location. Based on the marker protein signals, cells were annotated into 16 distinct cell types. These included neoplastic cells (cancer cells), endothelial cells, and an array of immune cell types: $CD163^+$ macrophages (M2Mac), $CD163^-$ macrophages (M1Mac), $CD8^+$ T cells (Tc), $CD4^+$ helper T cells (Th), regulatory T cells (Treg), other T cells (Tother), classical monocytes (Cl Mo), non-classical monocytes (non-Cl Mo), intermediate monocytes (Int Mo), natural killer cells (NK), dendritic cells (DC), mast cells, neutrophils, and undefined immune cells (Undefined). The clinical data for the LUAD patients include age (>75 and ≤75), sex (female and male), Body Mass Index BMI (>30 and ≤30), smoking status (smoking and non-smoking), stage (early: I-II and late: III-IV), and histological subtypes (lepidic, papillary, acinar, micropapillary, and solid).

Calculation of cell density and proportional fractions of cells in each IMC image

For the 16 distinct cell types identified in each IMC image, we quantified two key parameters: cell density and cell fraction. The cell density (D_i) for cell type i in an image was calculated as the cell count per megapixel. We computed two types of cell fractions for each image. The overall cell fraction (F_i^{all}) for each cell type i was established by its proportion relative to the total count of all 16 cell types. The immune cell fraction (F_i^{imm}) for each immune cell type i was determined by its ratio to the sum of the 14 immune cell types.

Calculation of proximity score between each pair of cell types

To quantify the proximity from cell type X to cell type Y (X→Y) within an IMC image, we established a multi-step analytical procedure. First, for each Y cell, we computed the minimum distance to the nearest X cell, resulting in a distance vector {d1, d2, …, dn}, where n signifies the total number of Y cells within the image. Second, we converted the distribution of these distances into a cumulative function reflecting the proximity of X cells to Y cells.

Considering that only cells within a specific range are likely to engage in functional interactions, we excluded distances that were greater than a threshold. In this study, we set the distance threshold as ten times the average cancer cell diameter. Further, a cumulative distribution function was constructed where the X-axis represents the minimum distances {d1, d2, ..., dn} from each Y cell to the nearest X cell, and the Y-axis indicates the cumulative proportion of Y cells for which the distance is less than or equal to a given distance on the X-axis. Finally, we calculated the area under the cumulative function to measure the proximity of X→Y. The proximity score (X→Y) provides a value between 0 and 1, where a higher value denotes closer proximity of X cells to Y cells. As a quality control step, any IMC image with fewer than ten reference Y cells is labeled 'NA' (Not Applicable) and omitted from further analysis. It is crucial to note that by this metric, proximity is inherently asymmetric. Namely, the proximity X→Y is generally not equal to the proximity Y→X.

Categorization of immune cells based on their proximity to M2 macrophages in IMC images

Considering the potential influences of certain immune cell types (e.g., B, Th, and Tc cells), we delineated the cells in an IMC image based on the presence of M2 macrophages in their neighborhood, classifying them as either 'M2-proximal' or 'M2-distal'. For example, a Th cell was designated as 'M2-proximal' if the nearest M2Mac was within and including a 30 μm radius—corresponding to 30 pixels under the imaging parameters. In contrast, Th cells located beyond this threshold were identified as 'M2-distal'.

After defining M2-proximal and M2-distal B/Th/Tc cells, we calculated their overall cell fractions and immune cell fractions separately in each IMC image. The resultant fractions were correlated with patient prognosis. To ensure methodological rigor, we conducted a sensitivity analysis by adjusting the proximity radius from 10 to 100 pixels, aiming to validate the consistency of our findings across various spatial definitions.

Clustering of patients based on proximity scores

We conducted a hierarchical clustering analysis to discern patterns among LUAD patients using proximity scores for the 10 significant prognostic cell-to-cell interaction pairs. Utilizing the Complete-linkage clustering method, we clustered the patients based on their proximity metrics. Patients with missing values were omitted, resulting in a final cohort of 218 individuals. This cohort was stratified into two clusters—comprising 107 and 111 patients, respectively. The R package "*ComplexHeatmap*" was used to implement the clustering analysis with the complete linkage hierarchical clustering method.

Identification of clinical factors correlated with cell proximity

We employed a multivariable linear regression model to investigate the association between clinical parameters and the ten cell-cell proximity scores linked to prognostic outcomes. Specifically, the following model was used:

$$Proximity \sim Age + Sex + BMI + Smoking + Stage + Histological\ Subtype$$

For this analysis, the significance (p-value) and effect size (β coefficient) for each clinical factor were calculated to discern their respective correlations with the proximity scores. Reference categories were established for the variables: 'Age' (≤75 years), 'Sex' (Male), 'BMI' (≤30), 'Smoking' (Non-smoking), 'Stage' (Early: I-II), and 'Histological Subtype' (Lepidic), to facilitate the interpretation of the regression coefficients.

Quantifying molecular interaction influence on cell proximity

To discern the extent to which molecular interactions influence cell-cell proximity, we adopted a randomization procedure by shuffling the cell type labels within each IMC image. Specifically, for each IMC image, we randomly relabeled the types of all cells while preserving the total counts per cell type. After reshuffling, we recalculated the proximity scores for all cell-cell pairs. This process was repeated 100 times to establish a null distribution for proximity scores. This null model provided a baseline to determine the extent of deviation exhibited by the actual cell arrangements.

The normalized proximity scores were computed as the standard scores (Z-scores) for the original proximity scores against this null distribution. By normalization, we removed the influence of cell densities on proximity scores. A positive Z-score indicates that the observed proximity between cell types X and Y exceeds that expected by random distribution, suggesting a propensity for interaction beyond what would be predicted by cell density alone. Conversely, a negative Z-score implies a separation between cell types X and Y greater than that of the null model, potentially indicating inhibitory interactions or spatial exclusion. These normalized scores thus serve as indicators of the specific contributions of molecular interactions to cell-cell proximity within the tissue microenvironment.

Survival analysis

Univariable Cox regression analysis was used to determine the association between proximity scores and patient overall survival in the LUAD IMC cohort. Multivariable Cox regression analysis was subsequently applied to further investigate the prognostic association

while adjusting for clinical factors including age, sex, stage, and histological subtype. Smoking status and BMI were found not significantly associated with prognosis according to univariable analysis and therefore excluded from the multivariable analysis. Both univariable and multivariable Cox regression analyses were implemented by using the "coxph" function from the R package "*survival*". Kaplan-Meier survival curves were generated to visually contrast the stratified groups by using the R package "*survminer*".

Other statistical analysis

The Pearson correlation coefficient was calculated to estimate the correlation between different continuous variables, e.g., proximity scores and cell fraction. The partial correlation coefficient, implemented by using the R package "*ppcor*", was used to determine the relationship between two continuous variables after adjusting for a third factor. Comparative analyses between different sample groups were conducted using the "wilcox.test" function for the Wilcoxon rank-sum test. The Benjamini-Hochberg method was used to correct for multiple testing. We defined statistical significance as a p-value below 0.05, except where specifically indicated otherwise. All statistical procedures were executed within the R software environment (version 4.0.2).

Supplementary Information

The online version contains supplementary material available at https://doi.org/10.1186/s12943-024-02080-1.

Supplementary Material 1

Acknowledgements

This study is supported by the Cancer Prevention Research Institute of Texas (CPRIT) (RR180061 to CC) and the National Cancer Institute of the National Institute of Health (1R01CA269764 to CC). CC is a CPRIT Scholar in Cancer Research.

Author contributions

C.C.designed the concept and the method. C.C., V.S., and J.L. wrote the main manuscript text and prepared the figures. Y.L., X.W., and M.A. contributed to the preparation of figures and the manuscript. J.W., J.Z., and C.A. revised the manuscript and figures. All authors reviewed the manuscript.

Funding

This study is supported by the Cancer Prevention Research Institute of Texas (CPRIT) (RR180061 to CC) and the National Cancer Institute of the National Institute of Health (1R01CA269764 to CC).

Data availability

All data generated in this study, including calculated cell densities, cell fractions, and cell-cell proximity scores, is available at the repository: https://github.com/JRLi/CellPro/. The proximity calculation function, along with example data, is available for use at the repository: https://github.com/JRLi/GetCellPro. The original data utilized in this study were sourced from PMID: 36725934 (DOI: https://doi.org/10.5281/zenodo.7383627).

Declarations

Ethics approval and consent to participate

Not applicable.

Competing interests

The authors declare no competing interests.

Received: 3 June 2024 / Accepted: 6 August 2024
Published online: 04 September 2024

References

1. Flores R, Patel P, Alpert N, Pyenson B, Taioli E. Association of Stage Shift and Population Mortality among patients with Non-small Cell Lung Cancer. JAMA Netw Open. 2021;4(12):e2137508.
2. de Visser KE, Joyce JA. The evolving tumor microenvironment: from cancer initiation to metastatic outgrowth. Cancer Cell. 2023;41(3):374–403.
3. Kawai O, Ishii G, Kubota K, Murata Y, Naito Y, Mizuno T, et al. Predominant infiltration of macrophages and CD8(+) T cells in cancer nests is a significant predictor of survival in stage IV nonsmall cell lung cancer. Cancer. 2008;113(6):1387–95.
4. Parra ER, Zhang J, Jiang M, Tamegnon A, Pandurengan RK, Behrens C, et al. Immune cellular patterns of distribution affect outcomes of patients with non-small cell lung cancer. Nat Commun. 2023;14(1):2364.
5. Wortman JC, He TF, Solomon S, Zhang RZ, Rosario A, Wang R, et al. Spatial distribution of B cells and lymphocyte clusters as a predictor of triple-negative breast cancer outcome. NPJ Breast Cancer. 2021;7(1):84.
6. Fu T, Dai LJ, Wu SY, Xiao Y, Ma D, Jiang YZ, et al. Spatial architecture of the immune microenvironment orchestrates tumor immunity and therapeutic response. J Hematol OncolJ Hematol Oncol. 2021;14(1):98.
7. Giesen C, Wang HAO, Schapiro D, Zivanovic N, Jacobs A, Hattendorf B, et al. Highly multiplexed imaging of tumor tissues with subcellular resolution by mass cytometry. Nat Methods. 2014;11(4):417–22.
8. Sorin M, Rezanejad M, Karimi E, Fiset B, Desharnais L, Perus LJM, et al. Single-cell spatial landscapes of the lung tumour immune microenvironment. Nature. 2023;614(7948):548–54.
9. Speiser DE, Chijioke O, Schaeuble K, Münz C. CD4 + T cells in cancer. Nat Cancer. 2023;4(3):317–29.
10. Bied M, Ho WW, Ginhoux F, Blériot C. Roles of macrophages in tumor development: a spatiotemporal perspective. Cell Mol Immunol. 2023;20(9):983–92.
11. Mi H, Sivagnanam S, Betts CB, Liudahl SM, Jaffee EM, Coussens LM, et al. Quantitative spatial profiling of Immune populations in pancreatic ductal adenocarcinoma reveals Tumor Microenvironment heterogeneity and prognostic biomarkers. Cancer Res. 2022;82(23):4359–72.
12. Mi H, Ho WJ, Yarchoan M, Popel AS. Multi-scale spatial analysis of the Tumor Microenvironment reveals features of Cabozantinib and Nivolumab Efficacy in Hepatocellular Carcinoma. Front Immunol. 2022;13:892250.
13. Barua S, Fang P, Sharma A, Fujimoto J, Wistuba I, Rao AUK, et al. Spatial interaction of tumor cells and regulatory T cells correlates with survival in non-small cell lung cancer. Lung Cancer Amst Neth. 2018;117:73–9.
14. Chen J, Zhang K, Zhi Y, Wu Y, Chen B, Bai J, et al. Tumor-derived exosomal miR-19b-3p facilitates M2 macrophage polarization and exosomal LINC00273 secretion to promote lung adenocarcinoma metastasis via Hippo pathway. Clin Transl Med. 2021;11(9):e478.
15. Peranzoni E, Lemoine J, Vimeux L, Feuillet V, Barrin S, Kantari-Mimoun C, et al. Macrophages impede CD8 T cells from reaching tumor cells and limit the efficacy of anti-PD-1 treatment. Proc Natl Acad Sci U S A. 2018;115(17):E4041–50.

Publisher's Note